

2021-12-28

Copper Nanoparticles *In-Situ* Anchored on Nitrogen-Doped Carbon for High-Efficiency Oxygen Reduction Reaction Electrocatalyst

Hui-Fang Yuan

Yue Zhang

Xing-Wu Zhai

Li-Bing Hu

Recommended Citation

Gui-Xian Ge, Hui-Fang Yuan, Yue Zhang, Xing-Wu Zhai, Li-Bing Hu, Gui-Xian Ge, Gang Wang, Feng Yu, Bin Dai. Copper Nanoparticles *In-Situ* Anchored on Nitrogen-Doped Carbon for High-Efficiency Oxygen Reduction Reaction Electrocatalyst[J]. *Journal of Electrochemistry*, 2021, 27(6): 671-680.

POI: Peng Yu

Key Laboratory for Green Chemical Process of Xinjiang Corps, College of Chemistry and Chemical Engineering, Shihezi University, Shihezi 832005, Xinjiang, China, 3. Shihezi University Bingtuan Industrial Technology Research Institute Clean Energy Conversion and Storage Research Group, Shihezi 832005, Xinjiang, China, yufeng05@shu.edu.cn

Compared with noble metal platinum (Pt)-based catalysts, inexpensive non-noble metal electrocatalysts have attracted extensive attention for oxygen reduction reaction (ORR). Herein, chitosan as a kind of biomass resource rich in nitrogen and carbon was used to prepare nitrogen-doped carbon (N-C) and N-C

showed the high surface area of $607.3 \text{ m}^2 \cdot \text{g}^{-1}$ with the mean pore size of 2.5 nm and the pore volume of $0.40 \text{ cm}^3 \cdot \text{g}^{-1}$. The most positive Gibbs free energy change was the rate determining step for ORR process with the 4e mechanism, where the value of the Cu(111)/N-C(-0.39 eV) was lower than that of the N-C(-0.26 eV). The Cu/N-C exhibited superior onset and half-wave potentials (0.96 V and 0.84 V, respectively) in alkaline media ($0.1 \text{ mol} \cdot \text{L}^{-1}$ KOH), all of which are much better than those measured for N-C and commercial Pt/C. Furthermore, the Cu/N-C showed superior methanol crossover avoidance and oxygen reduction stability.

Available at: <https://jelectrochem.xmu.edu.cn/journal/vol27/iss6/11>

This Article is brought to you for free and open access by Journal of Electrochemistry. It has been accepted for inclusion in Journal of Electrochemistry by an authorized editor of Journal of Electrochemistry.

Copper Nanoparticles *In-Situ* Anchored on Nitrogen-Doped Carbon for High-Efficiency Oxygen Reduction Reaction Electrocatalyst

Authors

Hui-Fang Yuan, Yue Zhang, Xing-Wu Zhai, Li-Bing Hu, Gui-Xian Ge, Gang Wang, Feng Yu, and Bin Dai

Corresponding Author(s)

Feng Yu(yufeng05@mail.ipc.ac.cn);

Bin Dai(db_tea@shzu.edu.cn)

【Article】

DOI: 10.13208/j.electrochem.200724

Http://electrochem.xmu.edu.cn

氮掺杂碳原位锚定铜纳米颗粒用于 高效氧还原反应催化剂

袁会芳^{1#}, 张越^{1#}, 翟兴吾², 胡立兵¹, 葛桂贤²,
王刚¹, 于锋^{1,3*}, 代斌^{1*}

(1. 石河子大学化学化工学院, 新疆兵团绿色化工过程重点实验室, 新疆 石河子 832003; 2. 石河子大学理学院, 新疆 石河子 832003; 3. 石河子大学兵团工业技术研究院, 清洁能源转化与储存研究组, 新疆 石河子 832003)

摘要: 与贵金属铂基电催化氧还原反应(ORR)催化剂相比, 廉价的非贵金属催化剂引起了广泛的关注。本文以壳聚糖作为一种富含氮和碳元素的生物质资源, 利用碳溶法成功制备了氮掺杂碳原位负载铜纳米颗粒(Cu/N-C)催化剂。纯壳聚糖碳化得到的样品N-C的比表面积为 $67.5 \text{ m}^2 \cdot \text{g}^{-1}$ 、平均孔径 0.14 nm 、平均孔体积 $8.00 \text{ m}^3 \cdot \text{g}^{-1}$, 与之相比, Cu/N-C比表面积可达 $607.3 \text{ m}^2 \cdot \text{g}^{-1}$ 、平均孔径为 2.5 nm 、平均孔体积为 $0.40 \text{ cm}^3 \cdot \text{g}^{-1}$ 。通过密度泛函理论(DFT)进行计算表明, Cu(111)/N-C的自由能值低于N-C, 更有利于氧还原催化进行。在 $0.1 \text{ mol} \cdot \text{L}^{-1}$ KOH的介质中, Cu/N-C不仅表现出优异的起始和半波电势(分别为 0.96 V 和 0.84 V), 而且还表现出了优异的抗甲醇性能和稳定性, 并且Cu元素掺杂量达到 $1.67 \text{ wt.}\%$ 。

关键词: Cu/N-C; 壳聚糖; 生物质资源; 催化剂; 氧还原反应; 碳溶法

1 引言

面对全球变暖, 空气污染和资源短缺的严峻挑战, 科学家们将重点放在先进的清洁能源转换技术上, 包括燃料电池和太阳能电池^[1-4]。燃料电池是一种高效、环保的能量转换装置, 氧还原反应(oxygen reduction reaction, ORR)是一种缓慢的反应, 在燃料电池的应用中起着举足轻重的作用^[5-7]。因此, 使用合适的催化剂来提高ORR性能具有重要意义。到目前为止, 贵金属铂(Pt)基催化剂是最有效的ORR催化剂。然而, Pt基催化剂的应用仍然存在一些不可避免的问题, 例如成本高、稳定性差和甲醇中毒, 这些问题严重限制了燃料电池的大规模开发和商业化^[8-13]。为了解决这些问题, 至关重

要的是寻找低成本和高效率的催化剂作为Pt基催化剂的潜在替代品。

起初, 人们尝试制备非贵双金属 M_1 - M_2 催化剂($M_1, M_2 = \text{Fe}, \text{Co}, \text{Ni}$ 等过渡金属)。双金属合金作为电催化剂显示出优异的ORR性能^[14-17]。过渡金属可以与反应分子结合形成低势垒的过渡态, 降低活化能, 加速化学反应。2018年, Guan等^[18]采用双金属有机骨架(MOF)利用“双MOF杂化”约束热解策略制备了多孔的铁钴合金/氮掺杂碳(FeCo/N-C)纳米笼, 在 $0.1 \text{ mol} \cdot \text{L}^{-1}$ KOH溶液中, FeCo/N-C显示出优异的氧还原催化性能, 其半波电位达 $0.87 \text{ V}_{\text{RHE}}$ 略高于商用Pt/C(20%)电极。2019年, Xiong等^[19]以普鲁士蓝类似物(Prussian blue analogue, PBA)为前

引用格式: Yuan H F, Zhang Y, Zhai X W, Hu L B, Ge G X, Wang G, Yu F, Dai B. Copper nanoparticles *in-situ* anchored on nitrogen-doped carbon for high-efficiency oxygen reduction reaction electrocatalyst. *J. Electrochem.*, 2021, 27(6): 671-680.

收稿日期: 2020-07-24, 修订日期: 2021-02-18. #两位作者对此文章贡献相同.*通讯作者, Tel: (86-993)2057272, E-mail: yufeng05@mail.ipc.ac.cn; db_tea@shzu.edu.cn

国家自然科学基金项目(No. 21865025, No. 51962032)资助

驱体制备了Fe-Co双金属纳米粒子,在 $0.1 \text{ mol}\cdot\text{L}^{-1}$ NaOH中具有令人满意的半波电势,达到 $0.85 \text{ V}_{\text{RHE}}$,这与最新的商用Pt/C电催化剂相当。Yin等^[20]则采用静电纺丝法合成了嵌入N掺杂多孔碳纳米纤维包覆Fe-Co合金纳米粒子(Fe-Co@PCNF)。Fe-Co@PCNF在 $0.1 \text{ mol}\cdot\text{L}^{-1}$ KOH碱性和 $0.5 \text{ mol}\cdot\text{L}^{-1}$ H_2SO_4 溶液中均表现出相当于20wt.% Pt/C的ORR电催化活性,分别为 $0.854 \text{ V}_{\text{RHE}}$ 和 $0.739 \text{ V}_{\text{RHE}}$ 。

另一方面,铜由于其丰富储量和低成本,引起了人们的广泛关注^[21]。铜基材料对各种氧化或还原反应均表现出优异的电催化活性^[22, 23]。除了这些,据报道,当使用含有规则分布的N原子的聚合物代替普通的碳基材料作为载体的前体时,在退火过程中过渡金属与N原子之间化学键的产生要容易得多。这些催化剂在碳载体材料上的分散,沉积或掺杂大大提高了ORR活性^[24]。受此启发,Kang等人^[25]使用聚苯胺(polyaniline, PANI),一种众所周知的含N的导电聚合物^[26-29],吸附铜,然后通过退火制备Cu-NC催化剂,并且将由PANI衍生得到的Cu-NC催化剂输送到对ORR的催化活性。尽管已开发出各种基于铜的催化剂来提高ORR性能,但仍有很大的潜力去探索其他用于ORR的基于铜的催化剂。

众所周知,壳聚糖(chitosan, CTS)不仅由高含量的氮(6.89%)组成,而且还具有一些吸引人的特性,例如可持续、环保、低成本和无毒,受到了越来越多的关注^[30]。除了这些特性外,更重要的是在游离氨基和羟基中存在孤对电子,它们能够帮助CTS通过螯合机理与许多过渡金属离子具有很强的配位能力^[31]。此外,与传统的加热方法(traditional heating method, CHM)相比,碳浴法(carbon bath method, CBM)无需施加额外的保护性空气(例如 N_2 或Ar)即可达到与CHM相似的效果,因为碳能够在热解期间消耗氧气^[32]。

碳浴法是一种简便的策略,已被用于制备ORR的高活性催化剂。壳聚糖因其成本低,适用范围广而被用作氮和碳的前体^[28],而 $\text{Cu}(\text{NO}_3)_2\cdot 3\text{H}_2\text{O}$ 则用来提供Cu元素,所得的铜基碳材料应显示出高性能的ORR。本文通过一种便捷的碳浴法将Cu纳米颗粒成功地原位锚固在Cu,N掺杂碳(Cu-N-C)上,并且评估了所制备的铜基材料在碱性溶液中的电催化ORR行为。

2 实验

2.1 催化剂制备

所有化学品均为分析纯,无需进一步纯化即可使用。在典型的合成中,将壳聚糖(1 g)和 $\text{Cu}(\text{NO}_3)_2\cdot 3\text{H}_2\text{O}$ (0.64 g)的混合在200 mL烧杯中,利用磁力搅拌在室温下均匀分散在100 mL去离子水中,持续12 h。随后,将获得的混合物在 80°C 的烘箱中干燥。然后,最后将干燥的粉末放入50 mL的坩埚中,并放入150 mL的坩埚中,两个坩埚之间用碳粉填充。将坩埚在马弗炉中于 900°C 处理1 h。待温度降至室温时,将得到的黑色粉末用 $1 \text{ mol}\cdot\text{L}^{-1}$ HCl(200 mL)处理过夜,并用大量去离子水洗涤至中性。最后,在真空干燥箱中于 70°C 处理12小时后获得样品,最终样品命名Cu/N-C。

2.2 物化性能表征

用Cu K_3 辐射($\lambda = 1.5406 \text{ \AA}$)的 Brucker D 8 Advance X射线衍射仪记录了XRD(X-ray diffractometer, X射线衍射)图。X射线光电子能谱(X-ray photoelectron spectroscopy, XPS)数据由Amicus/ESCA 3400电子能谱仪记录。使用JEM-2100仪器(日本JEOL)收集透射电子显微镜(TEM),并在Tecnai G2 F20仪器(美国FEI)上收集高分辨率透射电子显微镜(high resolution transmission electron microscopy, HRTEM)图像。X射线光谱(EDS)作图图像在LEO 1430 VP STEM仪器(德国)上收集。在Micromeritics ASAP 2460仪器(美国乔治亚州诺克斯)中测试氮吸附-解吸等温线。计算了Brunauer-Emmett-Teller(BET)和Barrett-Joyner-Halenda(BJH)方法的比表面积、总孔体积和平均孔径。利用ICP(inductive coupled plasma emission spectrometer)电感耦合等离子体光谱仪测试了Cu元素的质量含量。取0.0137 g样品,定容25 mL溶液,稀释系数50,测试Cu元素含量。仪器读数 $0.4238 \text{ mg}\cdot\text{L}^{-1}$,换算测试结果为1.67wt.%。

2.3 电化性能评估

在CHI760E电化学工作站上测试了所有样品的催化活性。在充满 N_2 或 O_2 的三电极电解池下进行该过程。通过超声处理(30分钟)将5 mg催化剂粉末和25 μL 萘芬(5wt.%)和475 μL 无水乙醇混合以形成均相催化剂油墨,然后取10 μL 催化剂油墨涂抹到干燥后的玻璃碳电极上作为工作电极。此外,Ag/AgCl和Pt箔分别用作参比电极和对电极。在测试过程中,将 $0.1 \text{ mol}\cdot\text{L}^{-1}$ KOH溶液用作电解

质。在N₂或O₂饱和条件下以50 mV·s⁻¹的扫描速率进行循环伏安法(CV)测试,在O₂饱和条件下以400 r·min⁻¹至2500 r·min⁻¹的不同转速进行线性扫描伏安法(LSV)测试。在典型的ORR测试中,可以使用以下公式基于Koutecky-Levich(K-L)图的斜率来评估电子转移数:

$$1/J = 1/J_k + 1/(B\omega^{1/2}) \quad (1)$$

其中, J 是在RDE(rotating disc electrode, 转盘电极)上测得的电流密度, J_k 表示动电流密度, ω 表示电极转速, B 根据以下方程式表示:

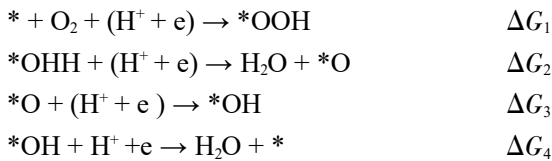
$$B = 0.2FC_0D_0\nu^{2/3}v^{-1/6} \quad (2)$$

其中, n 代表ORR程序中每个O₂分子的电子转移数, F 为法拉第常数(96485 C·mol⁻¹), C_0 为溶解的O₂浓度(1.2×10⁻³ mol·L⁻¹), D_0 为O₂扩散系数(1.9×10⁻⁵ cm²·s⁻¹), ν 是电解质运动粘度(0.01 cm²·s⁻¹)。

2.4 模拟计算

本章中所有的结构优化和能量计算都是VASP软件包中完成的,采用的是自旋极化密度泛函(DFT)方法^[33]。电子离子的相互作用由投影仪的增强波(PAW)伪势描述,交换相关能量由Perdew-Burke-Ernzerhof(PBE)函数在广义梯度逼近(GGA)中处理^[34,35]。我们分别为石墨N掺杂的石墨烯(N-C)和Cu/N-C的(111)平面(Cu(111)/N-C)构造了5×5×1和4×4×1超级电池。这些模型以3×3×1的网格为中心对伽马(gamma, Γ)点采样的布里渊区进行了几何优化。平面波的截止能量为450 eV。范德华(vander Waals)相互作用通过使用DFT-D3方法进行了描述^[26,36]。为了避免相邻的两个周期图像之间的相互作用,将真空层沿 z 方向设置为15。在结构优化期间,允许所有原子松弛,直到残余力和能量分别小于0.05 eV·Å⁻¹和10⁻⁴ eV。

根据计算的氢电极(CHE)模型,使用Norskov和他的同事提出的以下4e机理获得了N-C和Cu(III)/N-C每个氧还原反应(ORR)步骤的吉布斯自由能变化(ΔG)^[37]。



每个ORR步骤的 ΔG 通过 $\Delta G = \Delta E_{DFT} + \Delta E_{ZPE} - T\Delta S$ 计算获得,ORR过电势(η^{ORR})由下式确定: $G^{ORR} = \max[\Delta G_1, \Delta G_2, \Delta G_3, \Delta G_4], \eta^{ORR} = (G^{ORR}/e) + 1.23$ V。其中,*表示N-C和Cu(III)/N-C中的活性位, ΔE_{ZPE}

是可通过DFT计算直接获得的反应能差。 ΔE_{ZPE} 和 ΔS 分别是零点能量校正和室温($T = 298.15$ K)时的熵变化,这是通过振动频率分析计算得出的。CHE模型使用气相中H₂分子化学势的一半($\mu(H_2)$)作为质子电子对的化学势($\mu(H^+/e)$)为Cu/N-C,将纯壳聚糖通过相同处理获得N-C。

3 结果与讨论

3.1 形貌特征

通过X射线衍射图谱以确定复合材料的相组成和晶体结构。图1(A)显示了制备好的N-C(黑色曲线)和Cu/N-C(红色曲线)的XRD谱图。从XRD谱图中可见,这两个样品在~23.6°和~44°处显示出两个宽峰,分别对应于无序石墨峰和石墨碳平面(100)的衍射峰。此外,Cu/N-C在26.5°出现尖锐峰,这归因于(002)衍射的石墨碳(PDF#41-1487)。然而,在Cu/N-C中没有出现Cu基复合材料的衍射峰,表明Cu分散浓度太低而不能衍射。

为了分析ORR过程中Cu/N-C电极的动力学,解它们的电催化性能,通过TEM图像以研究N-C和Cu/N-C的形态和结构。从图1(A)可以看出,纯壳聚糖的N-C表现出明显的致密无定形碳结构。相比之下,如图1(B)所示,Cu/N-C表现出许多明显的孔。据报道,多孔结构的存在暴露了更多的活性位点,并促进了电解质的运输,从而导致了更好的ORR活性^[38]。通过测试N-C和Cu/N-C的高分辨率TEM(HRTEM)图像进一步分析。纯壳聚糖产生的N-C之间没有观察到任何层间间距(图1(C)),这表明,N-C在简单的热解后表现出无定形碳结构。此外,在用于Cu/N-C的HRTEM图像中(图1(D)),0.21 nm的层间距对应于Cu⁰(111)平面。以上这些结果证实了Cu金属存在于Cu/N-C中但不存在于N-C中,铜基材料对各种氧化或还原反应均具有出色的电催化活性。

通过STEM拍摄以进一步研究Cu/N-C的元素分布。如图1(E)表明,Cu、N、C和O元素均匀地分散在样品表面(Cu/N-C)。显然,Cu含量高于N含量。因此,推测在Cu/N-C中存在Cu金属,1 mol·L⁻¹ HCl处理过程中所吸附的O元素存在于Cu/N-C中。

通过氮孔隙率法测量以进一步研究所获得的N-C和Cu/N-C的结构特点。如表1所示,纯壳聚糖的N-C样品的BET表面积、孔体积和平均孔径分别为67.5 m²·g⁻¹、0.14 cm³·g⁻¹和8.00 nm。Cu/N-C的BET表面积(607.3 m²·g⁻¹)和孔体积(0.40 cm³·g⁻¹)明显

增加。Cu/N-C孔径为2.60 nm,小于N-C。而电催化过程中,催化部位的催化活性很大程度上取决于样品的BET表面积。

3.2 结构特征

3.2.1 拉曼光谱分析

通过拉曼光谱图研究了N-C和Cu/N-C的碳结构。D和G峰是由典型拉曼光谱中碳材料的缺陷位点和杂化 sp^2 碳键引起的。因此,碳材料的石墨化程度取决于D和G波段强度的比值(I_D/I_G)^[29]。通常, I_D/I_G 比越大,材料的石墨化程度越低^[30]。如图2(B)所示,N-C和Cu/N-C在拉曼光谱的 1339 cm^{-1} (D波段)和 1575 cm^{-1} (G波段)附近有两个突出的峰。N-C的 I_D/I_G 强度比为1.036,Cu/N-C的 I_D/I_G 值为1.056,这

表明N-C的缺陷率低高于Cu/N-C。此外,拉曼光谱中的二维峰是石墨烯的显著特征,其位置和形状可用于区分单层、双层或多层石墨烯。应当指出,两个样品中均存在2D峰,表明两个样品均显示出一定程度的石墨化,且Cu在一定程度上降低了石墨化。

3.2.2 X射线光电子能谱分析

通过X射线光电子能谱分析以进一步探索催化剂表面的化学组成。如图2(C)所示,Cu/N-C催化剂的Cu 2p光谱在931.9 eV和935.3 eV处显示两个峰,分别对应于 Cu^0 和 Cu^{2+} 电子态。但是,在N-C样品中无法检测到这两个峰。图2(D)显示,高分辨率的N-C的N 1s XPS光谱在397.9 eV、400.5 eV和404.3

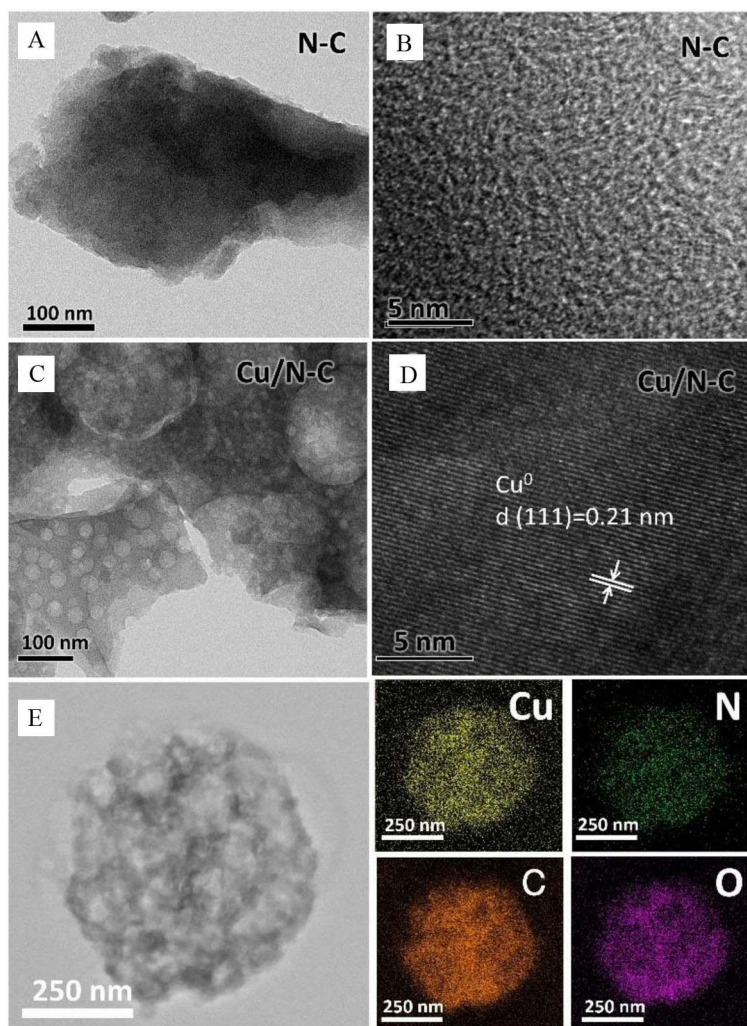


图1 (A) N-C和(C) Cu/N-C的TEM图像,(B) N-C和(D) Cu/N-C的HRTEM图像,(E) Cu/N-C: Cu, N, C, O的STEM图像和EDS元素映射图像。(网络版彩图)

Figure 1 TEM images of (A) N-C and (C) Cu/N-C. HRTEM images of (B) N-C and (D) Cu/N-C. (E) STEM image and EDS element mapping images of Cu/N-C: Cu, N, C and O. (color on line)

表1 N-C和Cu/N-C的特征

| Sample | Surface area/ ($\text{m}^2 \cdot \text{g}^{-1}$) | Pore volume/ ($\text{cm}^3 \cdot \text{g}^{-1}$) | Pore size/nm |
|--------|---|---|--------------|
| N-C | 67.5 | 0.14 | 8.00 |
| Cu/N-C | 607.3 | 0.40 | 2.60 |

eV处被解卷积为三个峰,分别归因于吡啶-N、吡咯-N和石墨-N。除了Cu/N-C的N1s XPS光谱中的上述三个峰外,还有一个清晰的Cu-N(399.5 eV)峰。过渡

金属络合物在碳载体材料上的分散、沉积或掺杂可大大增强ORR活性。因此,它通常对ORR具有良好的催化活性。如图2(E)所示,对氧元素峰的检查表明,Cu/N-C的高分辨率C 1s光谱分为C=C(284.4 eV)、C=N(285.4 eV)和O-C=O(288.2 eV)三个峰。但N-C出现了C=C(284.3 eV)和C=N(285.2 eV)的峰,没有O-C=O的峰。N-C的O 1s XPS峰(图2(F)) 532.6 eV、531.3 eV和530.2 eV峰,分别为吸附性O(O_{ad})、缺陷O(O_{def})和晶格O(O_{lat}),而Cu/N-C中缺乏晶格氧,因而说明没有 $\text{CuO}^{[39]}$ 存在。

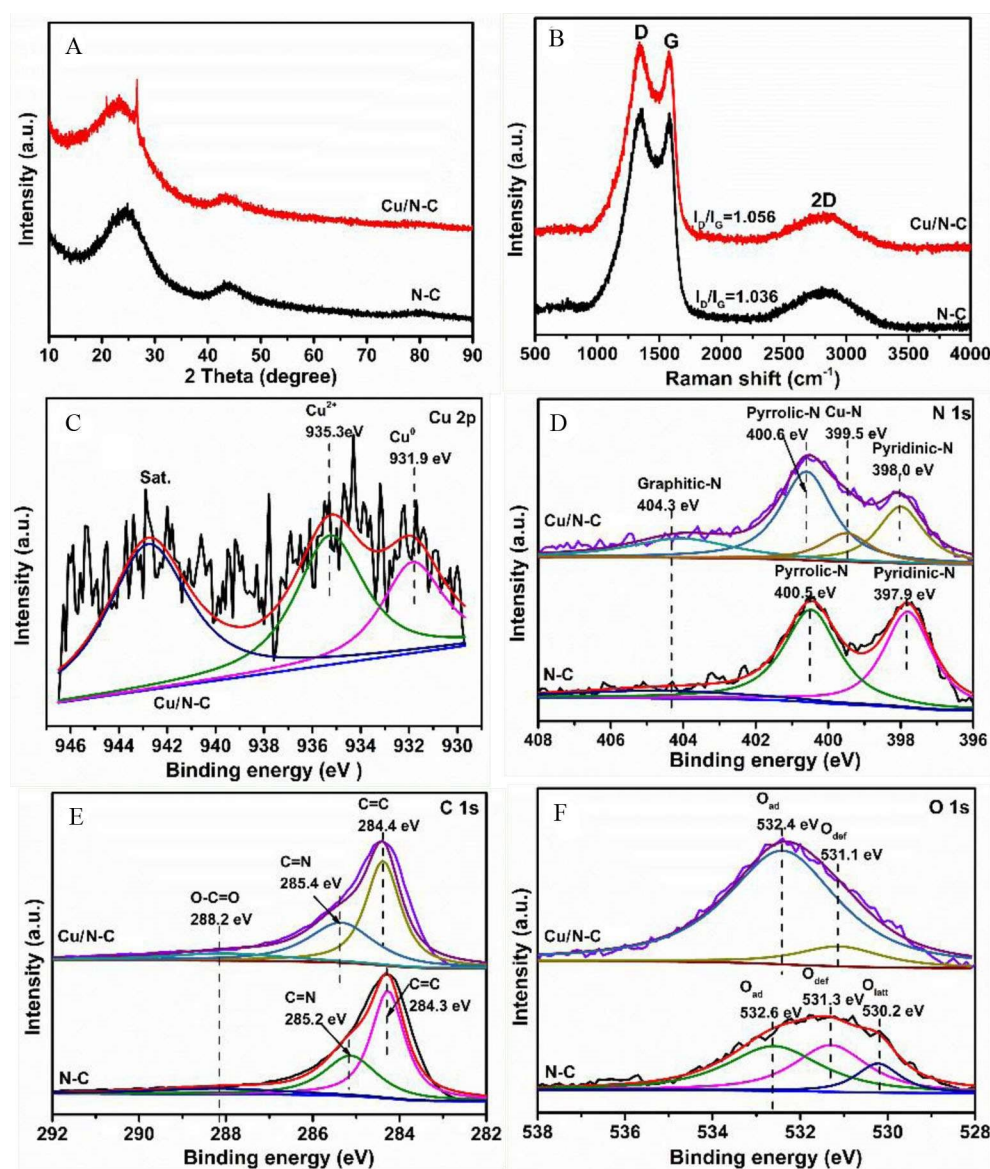


图2 (A) N-C和Cu/N-C的XRD谱图和(B)拉曼光谱;(C) Cu/N-C的高分辨率XPS谱图;元素(D) N 1s、(E) C 1s和(F) O 1s的XPS谱图。(网络版彩图)

Figure 2 (A) XRD patterns and (B) Raman spectra of N-C and Cu/N-C. (C) High resolution XPS spectra of Cu 2p for Cu/N-C. The fitted XPS spectra results of (D) N 1s, (E) C 1s and (F) O 1s for N-C and Cu/N-C. (color on line)

3.3 电化性能

首先在 $0.1 \text{ mol} \cdot \text{L}^{-1}$ KOH中, 通过CV和LSV测试Cu/N-C和N-C的ORR催化性能。如图3(A)所示, Cu/N-C在 $0.85 V_{\text{RHE}}$ 处有一个还原峰。相反, 在对应 N_2 饱和的溶液中未观察到电流响应的特征峰, 这表明Cu/N-C具有显著的ORR催化活性。在 O_2 饱和的 $0.1 \text{ mol} \cdot \text{L}^{-1}$ KOH中, 以 $1600 \text{ r} \cdot \text{min}^{-1}$ 的转速进行 $10 \text{ mV} \cdot \text{s}^{-1}$ 的线性扫描伏安法(LSV, 图3(B)), 以进一步评估Cu/N-C的ORR催化性能。为了比较, 还测试了N-C和市售的Pt/C(20wt.% J.M.)。Cu/N-C催化剂的起始电势(E_0)为 $0.96 V_{\text{RHE}}$, 半波电势($E_{1/2}$)为 0.84 , 比商用Pt/C催化剂的正电势更强($E_0 = 0.92 V_{\text{RHE}}$ 和 $E_{1/2} = 0.81 V_{\text{RHE}}$), 其结果与表2中列出的文献报道的结果相当。因此, 在碱性介质中, Cu/N-C具有比Pt/C更好的催化活性。无铜催化剂的ORR活性较差, 表明Cu的锚定可以提高ORR性能。

通过在 O_2 饱和溶液中以不同速度进行Cu/N-C的RDE伏安测试来分析ORR过程中Cu/N-C电极的动力学。结果表明, 电流密度随着速度的增加而增加(图3(C))。从图3(C)得出的各种电势下的相应Koutecky-Levich图(图3(D))在不同电势下显示出良好的线性, 这表明了相对于溶解氧浓度的一级反应动力学。斜率可以确定电子转移数(n)的不同电位下的K-L图。在图3(D)插图中, 在 0.25

V_{RHE} 、 $0.3 V_{\text{RHE}}$ 和 $0.35 V_{\text{RHE}}$ 的ORR测试中, 每个氧分子的Cu/N-C电极转移的电子数分别为3.81、3.84和3.86, 表明在Cu/N-C的催化作用下ORR遵循四电子转移途径。此外, 阻碍燃料电池应用的主要问题还包括催化耐久性, 因此, 我们在 O_2 饱和的 $0.1 \text{ mol} \cdot \text{L}^{-1}$ KOH水溶液中对Cu/N-C进行了计时安培耐久性评估。如图3(E)所示, 在12000 s后, Cu/N-C损失19.3%而Pt/C损失53.4%, 这表明商用Pt/C的耐久性低于Cu/N-C催化剂。因此, 具有优异活性和耐久性的Cu/N-C是一种有前途的非贵金属ORR催化剂, 可替代商用Pt/C催化剂。

燃料电池的另一个关键问题是耐甲醇性。通过添加 $2.0 \text{ mol} \cdot \text{L}^{-1}$ 甲醇(在100秒内)比较了Cu/N-C和Pt/C的交叉效应。Pt/C在添加甲醇后, 电流密度显著降低了55.1%(图3(F))。相比之下, Cu/N-C在电流密度(84.8%)下保持稳定的电流响应, 表明Cu/N-C的甲醇耐受性优于Pt/C。

3.4 理论模拟计算

电化性能表明, 与N-C相比, Cu(III)/N-C可以增强ORR的电催化活性。为了获得有关Cu(III)引入与ORR动力学之间关系的理论见解, 本工作通过DFT计算了N-C和Cu(III)/N-C上每个ORR步骤的吉布斯自由能 ΔG 。

如图4所示, 最大 ΔG 是采用4e机理进行ORR过程的速率确定步骤(RDS)的自由能。Cu(III)/N-C

表2 Cu/N-C与其他合金催化剂的比表面积和催化活性比较。可逆氢电极; 碱性溶液($0.1 \text{ mol} \cdot \text{L}^{-1}$ KOH); 酸性溶液($0.1 \text{ mol} \cdot \text{L}^{-1}$ HClO₄)

Table 2 Comparison of Cu/N-C with other alloy catalysts on specific surface area and catalytic activity. Reversible hydrogen electrode (RHE); Alkaline solution ($0.1 \text{ mol} \cdot \text{L}^{-1}$ KOH); Acidic solution ($0.1 \text{ mol} \cdot \text{L}^{-1}$ HClO₄)

| Catalyst | Surface area/ ($\text{m}^2 \cdot \text{g}^{-1}$) | Electrolyte | Onset potential/ V(vs. RHE) | Half-wave potential/ V(vs. RHE) | Ref. |
|---|---|-----------------|--------------------------------|------------------------------------|-----------|
| PtNi/C | 489 | Alkaline | - | 0.88 | [12] |
| PtFe alloy | - | Alkaline | 0.95 | 0.88 | [13] |
| Fe _{0.3} Co _{0.7} /NC | 52 | Alkaline | 0.98 | 0.88 | [18] |
| CoFe alloy | 745 | Alkaline | -- | 0.89 | [19] |
| FeCo@NC-750 | 42 | Alkaline | 0.94 | 0.80 | [16] |
| FeNi@NCNTs | 104 | Alkaline | 0.95 | 0.77 | [17] |
| DBD- FeCo@NC | - | Alkaline | 0.96 | 0.88 | [21] |
| FeCo@PCNF-800 | 304.98 | Alkaline/acidic | 0.94/0.84 | 0.85/0.74 | [20] |
| FeNi-NC | 1864 | Alkaline | 0.98 | 0.83 | [23] |
| Cu/N-C | 607.3 | Alkaline | 0.96 | 0.84 | This work |

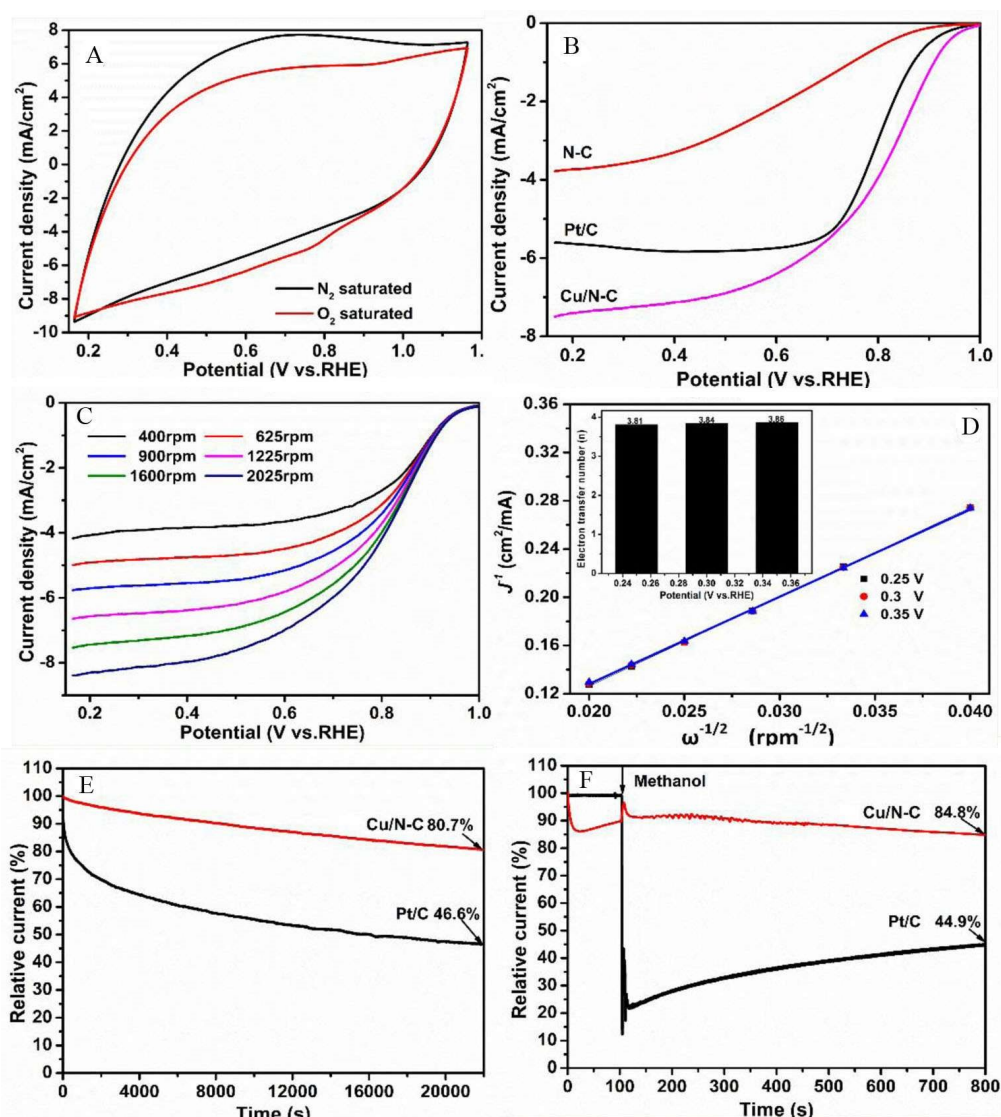


图3 (A) Cu/N-C在 $0.1 \text{ mol}\cdot\text{L}^{-1}$ KOH电解质中,扫描速率为 $50 \text{ mV}\cdot\text{s}^{-1}$ 时的CV曲线。(B) N-C、Cu/N-C和20wt.% Pt/C在 O_2 饱和的 $0.1 \text{ mol}\cdot\text{L}^{-1}$ KOH中的LSV曲线,转速为 $1600 \text{ r}\cdot\text{min}^{-1}$ 。(C) Cu/N-C在不同转速下的RDE伏安图。(D)相应的K-L图和Cu/N-C的电子转移数(插图)。(E) ORR阴极电流-时间($i-t$)法测定Cu/N-C和Pt/C的长期稳定性曲线和(F)对甲醇中毒的耐受性曲线。(网络版彩图)

Figure 3 (A) CV curves of Cu/N-C in $0.1 \text{ mol}\cdot\text{L}^{-1}$ KOH electrolyte at a scan rate of $50 \text{ mV}\cdot\text{s}^{-1}$. (B) LSV curves for N-C, Cu/N-C and 20wt.% Pt/C in O_2 -saturated $0.1 \text{ mol}\cdot\text{L}^{-1}$ KOH with a rotating speed of $1600 \text{ r}\cdot\text{min}^{-1}$. (C) RDE voltammograms of Cu/N-C at various rotation speeds. (D) Corresponding K-L plots and the electron transfer numbers (the inset) of Cu/N-C. (E) Long-term stability curves and (F) tolerance to methanol poisoning curves of Cu/N-C and Pt/C via the ORR cathodic current-time ($i-t$) method. (color on line)

(-0.39 eV)的最大 ΔG 低于N-C(-0.26 eV)的 ΔG ,即Cu(III)/N-C与N-C相比需要较低的电势来触发ORR过程。如图4(A)和4(B)所示,在N-C中引入Cu(III)后,每个基本步骤的 ΔG 均降低,并且ORR超电势从 0.97 V 降低至 0.84 V ,这是因为含氧中间体的吸附能增强了。因此,吉布斯自由能图和中间体的结构得到了优化,也就是说通过引入Cu(III),可以大大

提高Cu(III)/N-C的ORR催化活性。

4 结论

本工作将壳聚糖和 $\text{Cu}(\text{NO}_3)_2\cdot 3\text{H}_2\text{O}$ 的混合物通过一步碳浴法合成,经过 $1 \text{ mol}\cdot\text{L}^{-1}$ HCl处理后,最终获得了Cu/N-C催化剂。XPS发现Cu-N出现在Cu/N-C中,高分辨率的TEM图像和Cu 2p XPS光谱证实了 Cu^0 也存在于Cu/N-C中。结果表明,Cu和

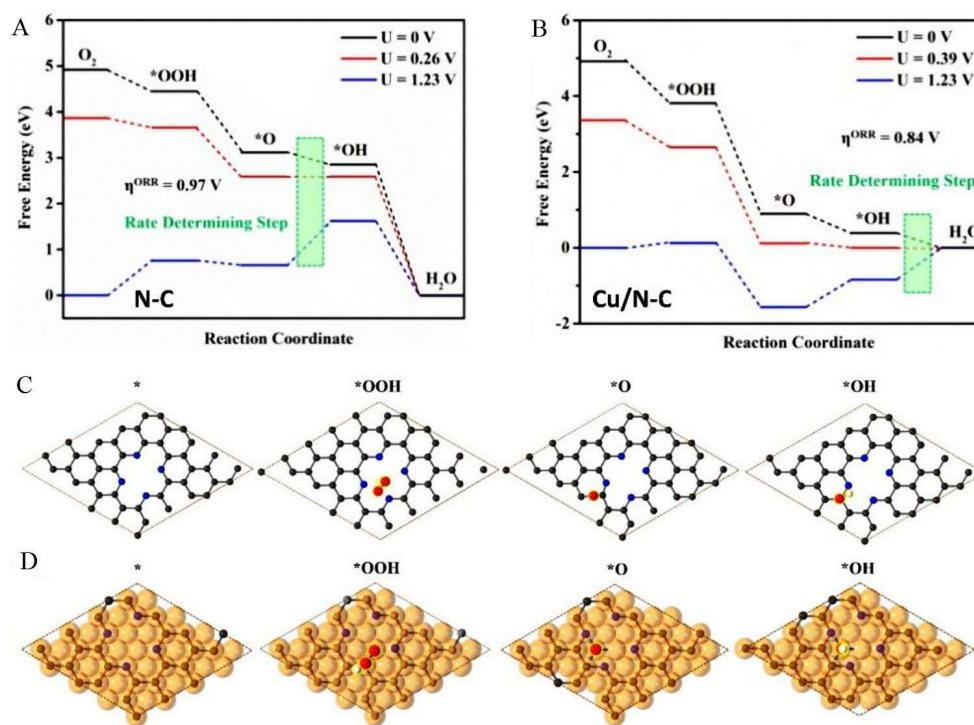


图4 DFT计算得到的(A) N-C和(B) Cu(111)/N-C上ORR的吉布斯自由能图。(C) N-C和(D) Cu(111)/N-C上ORR中间体的优化结构。灰色、白色、红色、蓝色和橙色分别代表碳、氢、氧、氮和铜原子。(网络彩图版)

Figure 4 Gibbs free energy diagrams of ORR on (A) N-C and (B) Cu(111)/N-C by DFT calculations. The optimized structures of the ORR intermediates on (C) N-C and (D) Cu(111)/N-C. Gray, white, red, blue and orange balls stand for the C, H, O, N and Cu atoms, respectively. (color on line)

Cu-N共同改善了Cu/N-C的氧还原催化性能。在 $0.1 \text{ mol} \cdot \text{L}^{-1}$ KOH中Cu/N-C催化剂表现出优异的ORR性能,它的起始电势(E_0)为 $0.96 \text{ V}_{\text{RHE}}$,半波电势($E_{1/2}$)为 $0.84 \text{ V}_{\text{RHE}}$ 。理论计算发现,引入Cu可以大大提高Cu/N-C的ORR催化活性。这项工作为通过一步碳浴法向能量转换合成新型的铜基碳材料提供了重要的指导。

参考文献(References):

- [1] Lu X F, Xia B Y, Zang S Q, Lou X W. Metal-organic frameworks based electrocatalysts for the oxygen reduction reaction[J]. *Angew. Chem. Int. Ed.*, 2019, 59(12): 4634-4650.
- [2] Mamtani K, Jain D, Dogu D, Gustin V, Gunduz S, Co A C, Ozkan U S. Insights into oxygen reduction reaction (ORR) and oxygen evolution reaction (OER) active sites for nitrogen-doped carbon nanostructures (CN_x) in acidic media[J]. *Appl. Catal. B - Environ.*, 2018, 220: 88-97.
- [3] Jia Q Y, Zhao Z P, Cao L, Li J K, Ghoshal S, Davies V, Stavitski E, Attenkofer K, Liu Z Y, Li M F, Duan X F, Mukerjee S, Mueller T, Huang Y. Roles of Mo surface dopants in enhancing the ORR performance of octahedral PtNi nanoparticles[J]. *Nano Lett.*, 2018, 18(2): 798-804.
- [4] Wang Y Q, Yu F, Zhu M Y, Ma C H, Zhao D, Wang C, Zhou A M, Dai B, Ji J Y, Guo X H. 3 N-Doping of plasma exfoliated graphene oxide via dielectric barrier discharge plasma treatment for the oxygen reduction reaction[J]. *J. Mater. Chem. A*, 2018, 6(5): 2011-2017.
- [5] Wang X Q, Li Z J, Qu Y T, Yuan T W, Wang W Y, Wu Y, Li Y D. Review of metal catalysts for oxygen reduction reaction: from nanoscale engineering to atomic design[J]. *Chem*, 2019, 5(6): 1486-1511.
- [6] Sun X, Atiyeh H K, Li M X, Chen Y. Biochar facilitated bioprocessing and biorefinery for productions of biofuel and chemicals: A review[J]. *Bioresour. Technol.*, 2020, 295: 122252.
- [7] Kim C, Dionigi F, Beermann V, Wang X L, Moller T, Strasser P. Alloy nanocatalysts for the electrochemical oxygen reduction (ORR) and the direct electrochemical carbon dioxide reduction reaction (CO₂ RR)[J]. *Adv. Mater.*, 2018, 31(SI): 1805617.

- [8] Chen M J, Hwang S, Li J Z, Karakalos S, Chen K, He Y H, Mukherjee S, Su D, Wu G. Pt alloy nanoparticles decorated on large-size nitrogen-doped graphene tubes for highly stable oxygen-reduction catalysts[J]. *Nanoscale*, 2018, 10(36): 17318-17326.
- [9] Wei Q L, Zhang G X, Yang X H, Chenitz R, Barham D, Yang L J, Ye S Y, Knights S, Sun S H. 3D porous Fe/N/C spherical nanostructures as high-performance electrocatalysts for oxygen reduction in both alkaline and acidic media[J]. *ACS Appl Mater. Inter.*, 2017, 9(42): 36944-36954.
- [10] Asset T, Chattot R, Fontana M, Mercier-Guyon B, Job N, Dubau L, Maillard F. A review on recent developments and prospects for the oxygen reduction reaction on hollow Pt-alloy nanoparticles[J]. *ChemPhysChem*, 2018, 19(13):1552-1567.
- [11] Yang H, Ko Y, Lee W, Zuttel A, Kim W. Nitrogen-doped carbon black supported Pt-M (M = Pd, Fe, Ni) alloy catalysts for oxygen reduction reaction in proton exchange membrane fuel cell[J]. *Mater. Today Energy*, 2019, 13: 374-381.
- [12] Zhang G R, Wollner S. Hollowed structured PtNi bifunctional electrocatalyst with record low total overpotential for oxygen reduction and oxygen evolution reactions[J]. *Appl. Catal. B - Environ.*, 2018, 222: 26-34.
- [13] Wang N N, Li Y Q, Guo Z L, Li H, Hayase S, Ma T L. Minute quantities of hexagonal nanoplates PtFe alloy with facile operating conditions enhanced electrocatalytic activity and durability for oxygen reduction reaction[J]. *J. Alloy. Compd.*, 2018, 752: 23-31.
- [14] Yu F, Liu M C, Ma C H, Di L B, Dai B, Zhang L L. A review on the promising plasma-assisted preparation of Electrocatalysts[J]. *Nanomaterials*, 2019, 9(10): 1436.
- [15] Martinez U, Babu S K, Holby E F, Chung H T, Yin X, Zelenay P. Progress in the development of Fe-based PGM-free electrocatalysts for the oxygen reduction reaction[J]. *Adv., Mater.*, 2019, 31(SD): 1806545.
- [16] Cai P W, Ci S Q, Zhang E H, Shao P, Cao C S, Wen Z H. FeCo alloy nanoparticles confined in carbon layers as high-activity and robust cathode catalyst for Zn-Air battery[J]. *Electrochim. Acta*, 2016, 220: 354-362.
- [17] Zhao X T, Abbas S C, Huang Y Y, Lv J Q, Wu M X, Wang Y B. Robust and highly active FeNi@NCNT nanowire arrays as integrated air electrode for flexible solid-state rechargeable Zn-Air batteries[J]. *Adv. Mater., Interfaces*, 2018, 5(9): 1701448.
- [18] Guan B Y, Lu Y, Wang Y, Wu M H, Lou X W. Porous iron-cobalt alloy/nitrogen-doped carbon cages synthesized via pyrolysis of complex metal-organic framework hybrids for oxygen reduction[J]. *Adv. Funct. Mater.*, 2018, 28(10): 1706738.
- [19] Xiong Y, Yang Y, DiSalvo F J, Abruna H D. Metal-organic-framework-derived Co-Fe bimetallic oxygen reduction electrocatalysts for alkaline fuel cells[J]. *J. Am. Chem. Soc.*, 2019, 141(27): 10744-10750.
- [20] Yin D D, Han C, Bo X J, Liu J, Guo L P. Prussian blue analogues derived iron-cobalt alloy embedded in nitrogen-doped porous carbon nanofibers for efficient oxygen reduction reaction in both alkaline and acidic solutions [J]. *J. Colloid Interface Sci.*, 2019, 533: 578-587.
- [21] Yan X Y, Tong X L, Zhang Y F, Han X D, Wang Y Y, Jin G Q, Qin Y, Guo X Y. Cuprous oxide nanoparticles dispersed on reduced graphene oxide as an efficient electrocatalyst for oxygen reduction reaction[J]. *Chem. Commun.*, 2012, 48(13): 1892-1894.
- [22] Cracknell J A, Vincent K A, Armstrong F A. Enzymes as working or inspirational electrocatalysts for fuel cells and electrolysis[J]. *Chem. Rev.*, 2008, 108(7): 2439-2461.
- [23] Solomon E I, Sundaram U M, Machonkin T E. Multicopper oxidases and oxygenases[J]. *Chem. Rev.*, 1996, 96(7): 2563-2605.
- [24] Zhao Y Y, Chu Y, Ju X P, Zhao J S, Kong L Q, Zhang Y, Carbon-supported copper-based nitrogen-containing supramolecule as an efficient oxygen reduction reaction catalyst in neutral medium[J]. *Catalysts*, 2018, 8(2): 53.
- [25] Pan Z F, An L, Zhao T S, Tang Z K. Advances and challenges in alkaline anion exchange membrane fuel cells [J]. *Prog. Energy Combust. Sci.*, 2018, 66: 141-175.
- [26] Kumar M N V R. A review of chitin and chitosan applications[J]. *React. Funct. Polym.*, 2000, 46(1): 1-27.
- [27] Qu J, Hu Q L, Shen K, Zhang K, Li Y L, Li H, Zhang Q R, Wang J Q, Quan W Q. The preparation and characterization of chitosan rods modified with Fe³⁺ by a chelation mechanism[J]. *Carbohydr. Res.*, 2011, 346(6): 822-827.
- [28] Wang L, Liu M C, Wang G, Dai B, Yu F, Zhang J L. An ultralight nitrogen-doped carbon aerogel anchored by Ni-NiO nanoparticles for enhanced microwave adsorption performance[J]. *J. Alloy. Compd.*, 2019, 776: 43-51.
- [29] Liu M C, Guo X H, Hu L B, Yuan H F, Wang G, Dai B, Zhang L L, Yu F. Fe₃O₄/Fe₃C@nitrogen-doped carbon for enhancing oxygen reduction reaction[J]. *ChemNanoMat*, 2018, 5(2): 187-193.
- [30] Yu H Y, Fisher A, Cheng D J, Cao D P. Cu,N-codoped hierarchical porous carbons as electrocatalysts for oxygen reduction reaction[J]. *ACS Appl. Mater. Inter.*, 2016, 8(33): 21431-21439.
- [31] Nie Y, Li L, Wei Z D. Recent advancements in Pt and

- Pt-free catalysts for oxygen reduction reaction[J]. Chem. Soc. Rev., 2015, 44(8): 2168-2201.
- [32] Guo D H, Shibuya R, Akiba C, Saji S, Kondo T, Nakamura J. Active sites of nitrogen-doped carbon materials for oxygen reduction reaction clarified using model catalysts[J]. Science, 2016, 351(6271): 361-365.
- [33] Borghei M, Lehtonen J, Liu L, Rojas O J. Advanced biomass-derived electrocatalysts for the oxygen reduction reaction[J]. Adv. Mater., 2018, 30(24): 1703691.
- [34] Yang L, Zeng X F, Wang D, Cao D P. Biomass-derived FeNi alloy and nitrogen-codoped porous carbons as highly efficient oxygen reduction and evolution bifunctional electrocatalysts for rechargeable Zn-air battery[J]. Energy Stor. Mater., 2018, 12: 277-283.
- [35] Rinaudo M. Chitin and chitosan: Properties and applications[J]. Prog. Polym. Sci., 2006, 31(7): 603-632.
- [36] Huang C L, Zhang H Y, Sun Z Y, Liu Z M. Chitosan-mediated synthesis of mesoporous α -Fe₂O₃ nanoparticles and their applications in catalyzing selective oxidation of cyclohexane[J]. Sci. China. Chem., 2010, 53(7): 1502-1508.
- [37] Guibal E. Heterogeneous catalysis on chitosan-based materials: a review[J]. Prog. Polym. Sci., 2005, 30(1): 71-109.
- [38] Huang J Y, Liang Y R, Hu H, Liu S M, Cai Y J, Dong H W, Zheng M T, Xiao Y, Liu Y L. Ultrahigh-surface-area hierarchical porous carbon from chitosan: acetic acid mediated efficient synthesis and its application in superior supercapacitors[J]. J. Mater. Chem. A, 2017, 5(47): 24775-24781.
- [39] Hu L B, Wei Z X, Yu F, Yuan H F, Liu M C, Wang G, Peng B H, Dai B, Ma J M. Defective ZnS nanoparticles anchored *in situ* on N-doped carbon as a superior oxygen reduction reaction catalyst[J]. J. Energy. Chem., 2019, 39: 152-159.

Copper Nanoparticles *In-Situ* Anchored on Nitrogen-Doped Carbon for High-Efficiency Oxygen Reduction Reaction Electrocatalyst

Hui-Fang Yuan^{1#}, Yue Zhang^{1#}, Xing-Wu Zhai², Li-Bing Hu¹, Gui-Xian Ge²,
Gang Wang¹, Feng Yu^{1,3*}, Bin Dai^{1*}

(1. Key Laboratory of Green Chemical Process of Xinjiang Corps, College of Chemistry and Chemical Engineering, Shihezi University, Shihezi 832003, Xinjiang, China; 2. School of Science, Shihezi University, Shihezi 832003, Xinjiang, China; 3. Shihezi University Bingtuan Industrial Technology Research Institute Clean Energy Conversion and Storage Research Group, Shihezi 832003, Xinjiang, China)

Abstract: Compared with noble metal platinum (Pt)-based catalysts, inexpensive non-noble metal electrocatalysts have attracted extensive attention for oxygen reduction reaction (ORR). Herein, chitosan as a kind of biomass resource rich in nitrogen and carbon was used to prepare nitrogen-doped carbon (N-C) and N-C *in-situ* anchored by copper nanoparticles (Cu/N-C). The as-obtained N-C and Cu/N-C nanoparticles were successfully used as non-noble electrocatalysts tested for ORR. Compared with the N-C, the Cu/N-C showed the high surface area of 607.3 m²·g⁻¹ with the mean pore size of 2.5 nm and the pore volume of 0.40 cm³·g⁻¹. The most positive Gibbs free energy change was the rate determining step for ORR process with the 4e mechanism, where the value of the Cu (111)/N-C(-0.39 eV) was lower than that of the N-C(-0.26 eV). The Cu/N-C exhibited superior onset and half-wave potentials (0.96 V and 0.84 V, respectively) in alkaline media (0.1 mol·L⁻¹ KOH), all of which are much better than those measured for N-C and commercial Pt/C. Furthermore, the Cu/N-C showed superior methanol crossover avoidance and oxygen reduction stability.

Key words: Cu/N-C; chitosan; biomass resource; electrochemical catalyst; oxygen reduction reaction; carbon-bath method